The synthesis and biological applications of photo-activated ruthenium anticancer drugs

Lameijer, L.N.

Chapter 6:

Efficient red light-activation of a NAMPT inhibitor under hypoxia using water-soluble ruthenium complexes

Abstract: Two water-soluble ruthenium complexes [**1**]Cl_2 and [**2**]Cl_2 are described that release a cytotoxic nicotinamide phosphoribosyltransferase (NAMPT) inhibitor upon irradiation with a low dose (21 J cm^{-2}) of red light. Up to an 18-fold increase in inhibition of NAMPT activity was measured upon red-light activation of [**2**]Cl_2, while no differences between activity in the dark and after irradiation were observed for [**1**]Cl_2. For the first time the dark and red light-induced cytotoxicity of these photocaged compounds could be tested on cells grown under hypoxic conditions (1% O_2). In skin (A431) and lung (A549) cancer cells a 3- to 4-fold increase in cytotoxicity was found upon red light irradiation for [**2**]Cl_2, when the cells were cultured and irradiated under normoxic conditions (21% O_2) or hypoxic conditions (1.0%). These results demonstrate the potential of photoactivated chemotherapy for hypoxic cancer cells where classical photodynamic therapy, which relies on oxygen activation, is poorly efficient.

This work has been published as a communication: L. N. Lameijer, D. Ernst, S. L. Hopkins, M. S. Meijer, S. H. C. Askes, S. E. Le Devedec, S. Bonnet, *Angew Chem Int Ed* **2017**, *56*, 11549-11553.

6.1 Introduction

Nicotinamide phosphoribosyltransferase (NAMPT) is a key enzyme in the salvage pathway of nicotinamide adenine dinucleotide (NAD^+) biosynthesis that is abnormally up regulated in cancer cells.[1] Importantly, high NAMPT expression in different types of cancer has been associated with poor prognosis in cancer patients, which makes NAMPT a potential therapeutic target.[2] It has been shown that NAMPT inhibition leads to reduction of intracellular NAD^+ levels, which can induce apoptosis in cancer cells.[2a, 3] However, it has also been reported that targeting of NAMPT might lead to side effects such as blindness.[4] A strategy called PhotoActivated ChemoTherapy (PACT) might solve selectivity issues.[5] PACT consists in hiding the toxicity of the compound with a caging agent that is released upon irradiation with light together with the free drug.[5b, 6] Ruthenium polypyridyl complexes are particularly promising photocaging groups as they can be activated using visible light,[7] whereas most organic caging groups require UV light for activation.[8] Unlike photodynamic therapy (PDT), a clinically approved therapy that relies on the photocatalytic activation of $^3O_2$ into $^1O_2$ by a photosensitizer,[9] PACT is oxygen independent[5b, 9] which makes it a promising and complementary therapeutic strategy for targeting hypoxic tumors. However, proof of efficacy of PACT under hypoxia is still lacking. Herein we describe a setup that can shine monochromatic red light on living cells under hypoxia (1%), allowing the study of PACT compounds [**1**]Cl_2 and [**2**]Cl_2 (Scheme 6.2). Red light is superior to previously reported blue- or green-light activation of PACT compounds due to deeper tissue penetration (0.5-1.0 cm),[10] and can be used with higher doses without significant light-induced cytotoxicity.[11] Two sterically hindered ruthenium photocaging scaffolds were chosen based upon earlier work by the groups of Turro and Kodanko:[12] $[Ru(tpy)(dmbpy)(L)]^{2+}$ (tpy = 2,2';6'-2"-terpyridine; dmbpy = 6,6'-dimethyl-2,2'-bipyridine) and $[Ru(tpy)(biq)(L)]^{2+}$ (biq = 2,2'-biquinoline). Both types of complexes have an absorption band that extends in the red region of the phototherapeutic window,[13] and photodissociate their ligand when the monodentate ligand L is a thioether or a pyridine moiety.[12a, 14] These scaffold were used to cage STF-31, a known cytotoxic organic compound containing a pyridine moiety, for which the toxicity was reported to originate from inhibition of both NAMPT enzyme activity[15] and glucose transporter 1 (GLUT1).[16] We synthesized the two STF-31-containing compounds [**1**]Cl_2 and [**2**]Cl_2 (Scheme 6.2), demonstrated that red light can release STF-31, and show that photorelease leads to efficient PACT under both normoxic (21% O_2), and hypoxic (1% O_2) conditions.

6.2 Results and discussion

STF-31 was synthesized according to a reported procedure [16b] using *t*-butylphenylsulfonyl chloride in the last step to install the *t*-butyl moiety (Scheme 6.1).

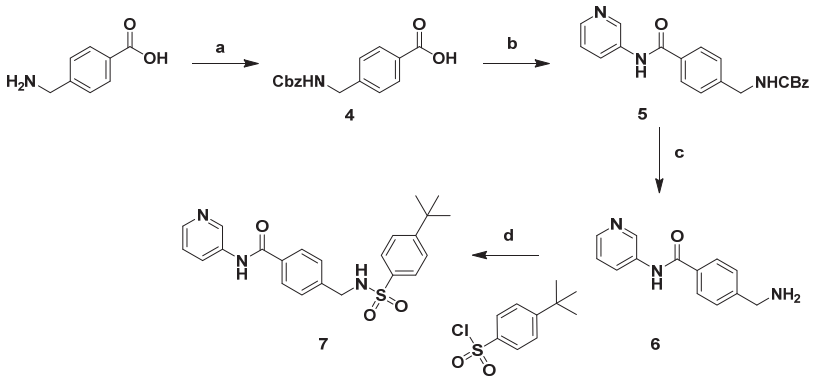

Scheme 6.1. a). CBz-Cl in water/dioxane/aq. $NaHCO_3$, 16 h, rt, 83%; b). i). cat. DMF, 1.65 eq. $(COCl)_2$ in THF, 5 h, rt – 50 °C ii). 1.06 eq. 3-aminopyridine in pyridine, 16 h, rt, 81%; c). 33% HBr in AcOH, 3 h, rt, 98%; d). 4-(*t*-butyl)benzenesulfonyl chloride in MeCN/pyridine, 16 h, rt, 54%.

Compounds [**1**]Cl_2 and [**2**]Cl_2 were then synthesized by reacting STF-31 with the precursors [Ru(tpy)(dmbpy)(Cl)]Cl[14] and [Ru(tpy)(biq)(Cl)]Cl, respectively (Scheme 6.2). The latter precursor was synthesized in high yield (90%), starting from ruthenium dimer [{Ru(tpy)Cl_2}$_2$].H_2O.[17] Both caged inhibitors were isolated as PF_6 salts, purified over Sephadex LH-20 and converted to their chloride salt by salt metathesis, to afford [**1**]Cl_2 and [**2**]Cl_2 as red or purple solids in 50% and 44% yield, respectively.

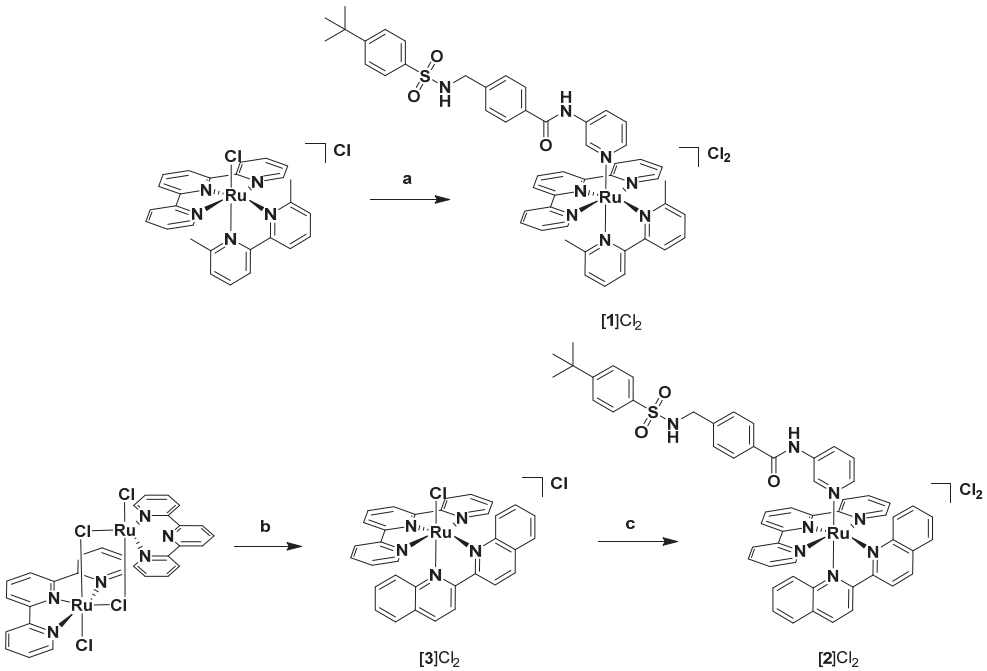

Scheme 6.2. a). i). STF-31 (2.0 eq.), $AgPF_6$ (2.2 eq.) in acetone/H_2O (2:1), 50° C, 2 h ii). NBu_4Cl in acetone, 44%; b). biq (1.0 eq.) in $(CH_2OH)_2$, 1 hr, 180 °C, 90%; c). i). STF-31 (1.2 eq.), $AgPF_6$ (2.1 eq.) in EtOH/H_2O (2:1), 80° C, 4 h; ii). NBu_4Cl in acetone, 50%

One of the challenges in PACT is to find the ideal balance between thermal stability and photoactivation efficiency, expressed as the photosubstitution quantum yield (Φ_P). Previous research has shown that $[Ru(tpy)(dmbpy)(SRR')]^{2+}$ complexes are less stable and more photoreactive than the corresponding $[Ru(tpy)(biq)(SRR')]^{2+}$ compounds in water,[18] therefore preventing their application in PACT.[19] In contrast, Turro et al. have demonstrated that complexes with L=pyridine are stable enough to be isolated while retaining photosubstitution properties under low-energy visible light (λ_{irr} > 590 nm).[12b] The photoreactivity of [**1**]Cl_2 and [**2**]Cl_2 in water was tested under red light irradiation. Figure 6.1 shows the evolution of the electronic absorption spectrum of $[\mathbf{1}]^{2+}$ upon activation at 625 nm under deoxygenated conditions in H_2O. The initial metal-to-ligand charge transfer (^{1}MLCT) band at 473 nm was gradually replaced by a new ^{1}MLCT band at 484 nm with a clear isosbestic point at 477 nm, due to the formation of $[Ru(tpy)(dmbpy)(H_2O)]^{2+}$ (*m/z* found 536.1, calc *m/z* 536.1 for $[Ru(tpy)(dmbpy)(OH)]^+$).

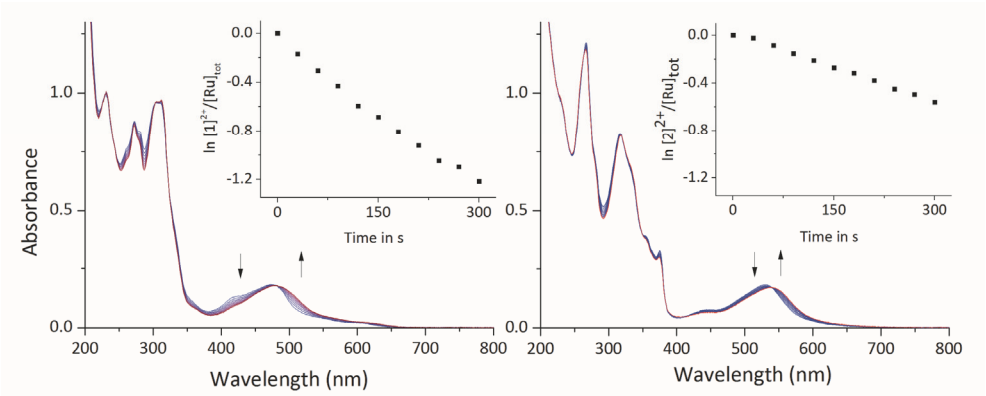

Figure 6.1. UV-vis spectra of [**1**]Cl_2 (left) and [**2**]Cl_2 (right) in deoxygenated H_2O under red light irradiation (625 nm, photon flux 1.30×10^{-7} mol.s^{-1}). Spectra were taken for 5 min each 30 s. T = 298 K.

In a parallel experiment using ^{1}H NMR spectroscopy a solution of [**1**]Cl_2 in D_2O was irradiated using white light (> 610 nm). During irradiation the doublet of at 6.89 ppm was replaced by two doublets at 6.80 and 7.78 ppm, while the characteristic ^{t}Bu singlet at 0.94 ppm disappeared, confirming photodissociation of STF-31 (Figure S.V.1). The photosubstitution quantum yields (Φ_{625}) were determined to be 0.057 at rt and 0.080 at 37 °C. Where the higher quantum yield for photosubstitution at increased temperature is consistent with thermal population of the triplet metal-centred states (^{3}MC) via the photochemically generated ^{3}MLCT states.[12b] For [**2**]Cl_2, irradiation at 625 nm resulted in a shift of the MLCT band at 531 nm to 549 nm, and the formation of the photoproduct $[Ru(tpy)(biq)(H_2O)]^{2+}$ (found *m/z* = 607.8, calcd *m/z* = 608.1 for $[Ru(tpy)(biq)(OH)]^+$). When a solution of [**2**]Cl_2 in D_2O was irradiated using white light (>610 nm) the ^{1}H NMR spectrum (Figure S.V.2) showed a new, distinctive quartet at 8.86 ppm, and a decrease of the doublet at 6.69 ppm and singlet at 0.90 ppm. Photosubstitution occurred with a quantum

yield Φ_{625} of 0.013 and 0.019 at rt and 37 °C, respectively (Table 6.1). The lower photoreactivity of [**2**]Cl_2 compared to [**1**]Cl_2 is consistent with previous work.[12b] Both [**1**]Cl_2 (log P_{ow} = -0.63 ± 0.04) and [**2**]Cl_2 (log P_{ow} = -0.08 ± 0.04) are water-soluble, but STF-31 is not (log P_{ow} = +3.92), resulting in ligand precipitation during photosubstitution of STF-31 in the NMR tube. Hence the caging Ru complexes significantly increase water solubility of the inhibitor.

Table 6.1. Absorption maxima (λ_{max}), molar absorption coefficients at λ_{max} (ε) and at 625 nm (ε_{625}), photosubstitution quantum yields (Φ_{625}) at 298 and 310 K in water, $^1O_2$ generation quantum yields (Φ_Δ) at 293 K, and photosubstitution reactivity ($\xi = \Phi_{625} \cdot \varepsilon_{625}$).

Complex	λ_{max} in nm[a] (ε in $M^{-1}cm^{-1}$)	ε_{625}[a] in $M^{-1}cm^{-1}$	Φ_{625}[a] (Φ_{625} at 310 K)	Φ_Δ[b]	ξ[20] (ξ at 310 K)
[**1**]Cl2	473 (8.1 x 10^3)	379	0.057 (0.080)	<0.005	2.2 (3.0)
[**2**]Cl2	531 (9.3 x 10^3)	609	0.013 (0.019)	0.036	0.79 (1.2)

[a] In H_2O. [b] In CD_3OD.

Before testing these compounds in cancer cells the dose of red light necessary to obtain full activation in the cell irradiation setup was evaluated to be 20.6 $J.cm^{-2}$, which corresponds to 10 minutes irradiation under normoxia (Figure 6.2).[11]

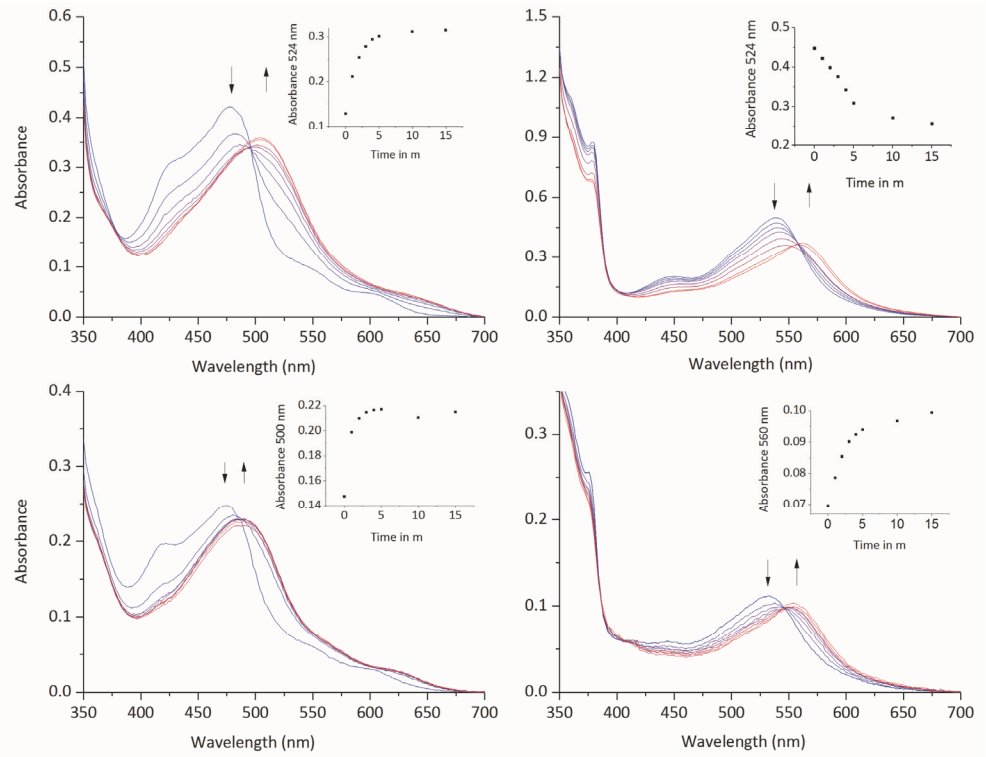

Figure 6.2. Irradiation of 1 x 10^{-4} M (v = 200 µL) [**1**]Cl_2 and [**2**]Cl_2 using the red light array for 15 minutes in the normoxia setup. Top left: [**1**]Cl_2 in DMSO. Top right: [**2**]Cl in DMSO. Bottom left: [**1**]Cl_2 in OptiMEM media + 10% DMSO. Bottom right: [**2**]Cl_2 in OptiMEM media + 10% DMSO. Irradiations were carried out over fifteen minutes. Spectra were plotted using Origin Pro 9.1 and the baseline was subtracted.

The cytotoxicity of STF-31 and of its caged analogues [**1**]Cl_2 and [**2**]Cl_2 was first tested in normoxic conditions (21% O_2) against three human cancer cell lines (A549, MCF-7, and A431) and a non-cancerous cell-line (MRC-5). [11] two plates were treated with STF-31, [**1**]Cl_2 or [**2**]Cl_2, and after 6 hours incubation one plate was irradiated with red light (628 nm, 20.6 J·cm^{-2}) while the other was left in the dark. At t = 48 h medium was replaced. Cell viability was then assayed by using sulforhodamine B (SRB) 96 h after seeding.[21] Cell growth inhibition effective concentrations (EC_{50}) were calculated from the dose-response curves of treated vs. non-treated wells (Figure 6.3 and Table S.V.1).

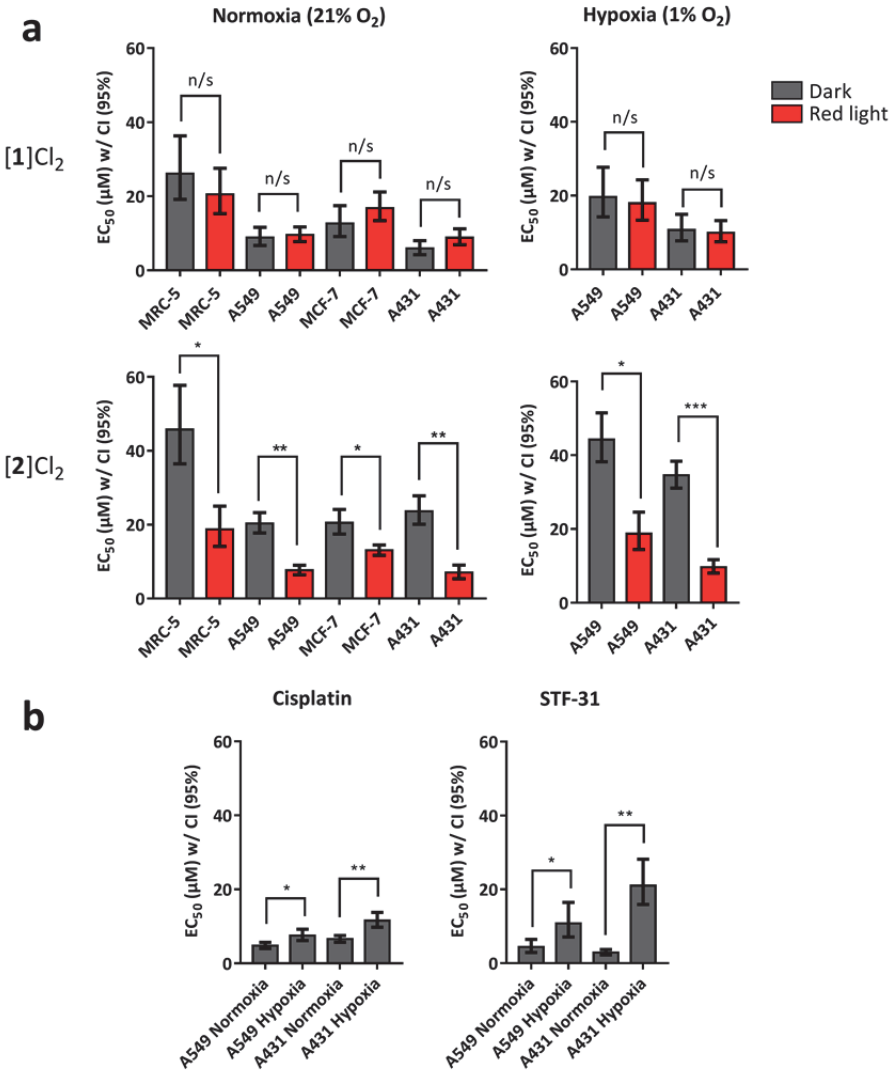

Figure 6.3. a). Cell growth inhibition effective concentrations (EC_{50} in μM) for **[1]**Cl_2, **[2]**Cl_2 in the dark and under red light irradiation in human cancer cells under normoxia (21.0% O_2, 7.0% CO_2) and hypoxia (1.0% O_2, 7.0% CO_2). **b).** EC_{50} for STF-31 and cisplatin under normoxia and hypoxia. Data points are the mean of three independent experiments; error bars show 95% confidence intervals (in μM). * = p ≤ 0.05, ** ≤ 0.01, *** ≤ 0.001. n/s = Not significant. See Table S.V.1 for all EC_{50} values.

Under normoxia (Figure 6.3a), STF-31 appeared to be highly cytotoxic in all cell lines, including MRC-5. Compound [**1**]Cl_2 also caused a great cytotoxic effect on all cancerous cell lines, but its effect was limited on the non-cancerous MRC-5 cell line (EC_{50} > 20 µM). Importantly, a negligible difference was found between the irradiated and non-irradiated wells. This result was in great contrast to [**2**]Cl_2, which was less cytoxic against the non-cancerous MRC-5 cells in the dark (EC_{50} > 40 µM) and highly toxic (EC_{50} < 10 µM) to cancerous cells after irradiation, with a marked difference in cytotoxicity between dark and irradiated cells for both A549 and A431. Considering the minimal $^1O_2$ production (3.6%, Table 6.1), this effect is most likely attributed to the anti-proliferative effect of the photoreleased STF-31.

To validate whether the photocytotoxicity could be ascribed to photorelease of STF-31, instead of PDT, [**1**]Cl_2, [**2**]Cl_2, and SFT-31, were tested under hypoxia, in which $^1O_2$ generation is impaired. We therefore modified our LED-based irradiation setup[11] allowing irradiation on living cells while controlling O_2 concentrations (1 - 21%, Figure S.V.4). We then repeated the cytotoxicity assay using the same protocol and light dose of 20.6 $J.cm^{-2}$, but now at 1.0% O_2 (see Figure S.V.4, lower left). As shown in Figure 6.2 and Table S.V.1, the EC_{50} values for all compounds were found to be higher than under normoxia, which is consistent with earlier reports on the higher resistance of hypoxic cells to chemotherapy.[22] No photocytotoxicity was observed for [**1**]Cl_2. However, the photoindices found for [**2**]Cl_2 under hypoxia (3.6 and 2.4 for A431 and A549 respectively) were identical to those found under normoxic conditions (3.3 and 2.6 for A431 and A549 respectively), demonstrating the observed photocytotoxicity for [**2**]Cl_2 is independent of the O_2 concentration.

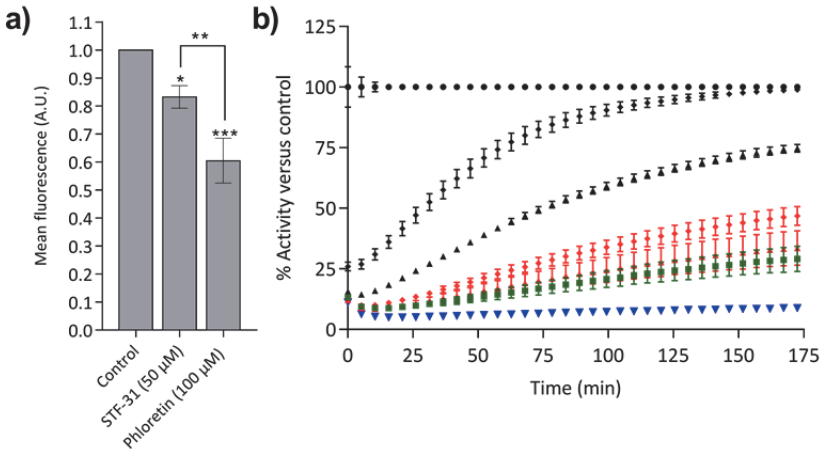

Figure 6.4. a). Normalized mean fluorescence intensity (MFI) of 2-[*N*-(7-nitrobenz-2-oxa-1,3-diazol-4-yl)amino]-2-deoxy-D-glucose (NBDG) in A549 cells treated with 2% DMSO, STF-31, or phloretin. Error bars are the mean of three independent experiments with ± standard deviation (SD). * = p ≤ 0.05, ** ≤ 0.01, *** ≤ 0.001. **b).** Representative plot of the percentage (%) of NAMPT activity observed for different compounds vs. control (2% DMSO) after 1 h incubation. Data points represent the mean of at least two replicates, and error bars represent standard error of the mean (SEM). ● = Vehicle control, ♦ = [2]Cl_2 dark (2 µM), ▲ = [1]Cl_2 dark (2 µM), ♦ = [2]Cl_2 light (2 µM), ▲ = [1]Cl_2 light (2 µM), ■ = STF-31 (2 µM), ▼ = FK866 (20 µM).

We then investigated the enzyme inhibition properties of STF-31, which is both a reported GLUT-1 and NAMPT inhibitor.[15a, 16a, 23] GLUT-1 overexpressing A549 cells[24] were starved using glucose-free medium, followed by incubation of 2 h with a vehicle control (2% DMSO), 50 µM STF-31, or 100 µM phloretin, a well-known GLUT-1 inhibitor.[25] Cells were then treated with the fluorescent D-glucose analogue NBDG,[26] and analyzed by flow cytometry (Figure S.V.6). STF-31 showed a minimal glucose-uptake inhibition compared to phloretin.[27] Therefore the observed cytotoxicity of STF-31 is most likely not related to impaired glucose uptake and GLUT-1 inhibition. The NAMPT enzyme activity inhibition of STF-31, [**1**]Cl_2, and [**2**]Cl_2, was therefore determined using the commercial Cyclex® assay after 1 h incubation of A549 cells with the irradiated or non-irradiated compounds (Figure 6.4b). At 2 µM concentration STF-31 showed the largest effect on NAMPT activity, confirming that it is a NAMPT inhibitor.[15a] Use of [**2**]Cl_2 resulted in a dramatic reduction in NAMPT activity after red light activation, whereas the non-irradiated sample suffered much less inhibition. A similar effect was observed for [**1**]Cl_2, although the dark activity was found to be much higher than that of [**2**]Cl_2. The dark inhibitory concentrations (IC_{50}) of 4.8 µM for [**2**]Cl_2 was lowered by a factor 18 down to 0.26 µM after irradiation, which is similar to the value obtained for STF-31 (0.25 µM). The NAMPT inhibitory effect of STF-31 is thus fully recovered upon red-light activation of [**2**]Cl_2.

Table 6.2. NAMPT activity inhibitory concentration (IC_{50} with 95% confidence intervals, in µM) obtained for STF-31, **[2]**Cl_2 in the dark and [**2**]Cl_2 after red light irradiation. Photoindex (PI) = $IC_{50,dark}/IC_{50,light}$.

STF-31		[**2**]Cl_2				
IC_{50} in µM (Dark)	CI	IC_{50} in µM (Dark)	CI	IC_{50} in µM	CI	PI
0.25	+0.027 -0.027	4.8	+0.89 -0.75	0.26	+0.079 -0.094	18

[a] Samples were irradiated for 10 minutes at 37 °C. See appendix V.

The almost identical EC_{50} values found for [**1**]Cl_2 in the dark and after light irradiation, and its high NAMPT inhibition in the dark, suggested that [**1**]Cl is thermally unstable: Monitoring for 48 hours at 37 °C in the dark in OptiMEM® (Figure 6.5), showed that [**1**]$^{2+}$ slowly decomposes to [Ru(tpy)(dmbpy)(OH_2)]$^{2+}$ while [**2**]$^{2+}$ remains stable (Figure S.V.7, left and right). This result is in contrast to the report of Kodanko et al. who used [Ru(tpy)(dmbpy)]$^{2+}$ to cage a steroidal CYP17A1 inhibitor.[12a] According to our results, [Ru(tpy)(N-N)(L)]$^{2+}$ complexes are only stable enough for PACT when the bidentate ligand is 2,2'-biquinoline, whereas ligands which induce increased steric strain, such as 6,6'-dimethyl-2,2'-bipyridine increase the photoreactivity but also the thermal lability.[14]

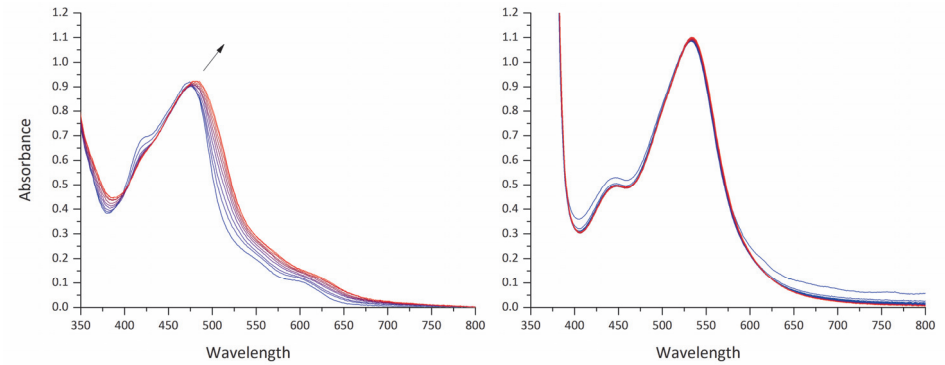

Figure 6.5. Stability of [**1**]Cl_2 (left) and [**2**]Cl_2 (right) in OptiMEM media + 2.5% FCS at 37 °C over 48 hours in the dark. Spectra measured each hour, gradient indicates intervals from blue to red. Arrow (left) indicates a shift of the MLCT absorption maximum due to formation of the chlorido species.

6.3 Conclusion

In conclusion, we have demonstrated for the first time the potential of PACT in hypoxic cancer cells using a photocaged NAMPT inhibitor. Whereas under hypoxic conditions classical PDT type II would not be effective because of the absence of dioxygen, [**2**]Cl_2 represents a promising form of photocaged drug, with a similar photoindex under hypoxia (1% O_2) as in normoxia (21% O_2). Also, this compound is soluble in water and can be activated using red light, whereas most PACT compounds reported to date require UV, blue or green light. The steric hindrance of [**2**]Cl_2 is high enough to obtain activation using clinically relevant light doses (21 $J.cm^{-2}$),[28] but low enough to acquire thermal stability. In contrast, [**1**]Cl_2 is too labile in the dark, which make it unsuitable for PACT. Altogether this study represents the first example of PACT where the phototoxicity index measured in hypoxic cancer cells with red light can be explained altogether by a low $^1O_2$ quantum yield, an efficient oxygen-independent photosubstitution reaction, and an enzyme inhibition assay.

6.4 Experimental

6.4.1 General

Reagents were purchased from Sigma-Aldrich and used without further purification. Dry solvents were collected from a Pure Solve MD5 solvent dispenser from Demaco. For all inorganic reactions solvents were deoxygenated by bubbling argon through the solution for 30 minutes. Flash chromatography was performed on silica gel (Screening devices B.V.) with a particle size of 40 - 64 µM and a pore size of 60 Å. TLC analysis was conducted on TLC aluminium foils with silica gel matrix (Supelco, silica gel 60, 56524) with detection by UV-absorption (254 nm). Infrared spectra were recorded on a Perkin Elmer UATR (Single Reflection Diamond) Spectrum Two device (4000-700 cm^{-1}; resolution 4 cm^{-1}). ^1H NMR and ^{13}C NMR were recorded in [D_6]DMSO and CD_3OD with chemical shift (δ) relative to the

solvent peak on a Bruker AV-500. High resolution mass spectra were recorded by direct injection (2 µl of 2 µM solution in water/acetonitrile; 50/50; v/v and 0.1% formic acid) in a mass spectrometer (Thermo Finnigan LTQ Orbitrap) equipped with an electrospray ion source in positive mode (source voltage 3.5 kV, sheath gas flow 10, capillary temperature 250 °C) with resolution R = 60000 at m/z 400 (mass range m/z = 150 – 2000) and dioctylphtalate (m/z = 391.28428) as a lock mass. The high-resolution mass spectrometer was calibrated prior to measurements with a calibration mixture (Thermo Finnigan). Elemental analysis was performed at Kolbe Mikrolab Germany to confirm the purity of STF-31, [**1**]Cl_2 and [**2**]Cl_2 ≥ 95%.

6.4.2 Ligand synthesis

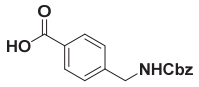

4-[(Benzyloxycarbonyl)amino]methyl benzoic acid, 4: To a cooled mixture (0 °C) of 4-(aminomethyl)benzoic acid (10.0 g, 66.2 mmol) in water/dioxane/aq. $NaHCO_3$ (700 ml, 5:1:1, 0.09 M) was added dropwise benzyl chloroformate (11.3 mL, 79.2 mmol). The reaction was allowed to reach room temperature and stirred overnight after which 1 M HCl was added until a pH of ~3 was reached. The resulting suspension was filtered, washed with water (3 x 100 mL) and Et_2O (3 x 100 mL) affording the title compound as a white powder (15.7 g, 55.0 mmol, 83%). R_f = 0.85 (10% H_2O in EtOAc); IR (neat): 3310, 3032, 2948, 2676, 1683, 1611; ^{1}H NMR: (500 MHz, [D_6]DMSO) δ = 12.89 (s, 1H, COO*H*), 7.90 (t, J = 7.1 Hz, 3H, H_{arom}), 7.37 (d, J = 4.7 Hz, 6H, H_{arom}), 5.05 (s, 2H, CH_2 Cbz), 4.27 (d, J = 6.4 Hz, 2H, CH_2 Arom). ^{13}C NMR (126 MHz, [D_6]DMSO) δ = 167.7 (C=O *CO*OH), 157.0 (C=O CBz), 145.4 (C_q Arom), 137.6 (C_q Arom), 129.9 (C_q Arom), 129.9 (C_H Arom), 128.9 (C_H Arom), 128.4 (C_H Arom), 128.3 (C_H Arom), 127.5 (C_H Arom), 66.0 (CH_2 CBz), 44.2 (CH_2 Arom); HRMS: *m/z* calcd for [$C_{16}H_{15}NO_4$ + H^+]: 286.10738; found: 286.10756.

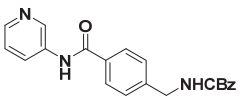

Benzyl (4-(pyridin-3-ylcarbamoyl)benzyl)carbamate, 5: To a solution of **4** (10.7 g, 37.5 mmol) in dry THF (150 mL, 0.25 M) at rt was added a catalytic amount of DMF (five drops) followed by the dropwise addition of $(COCl)_2$ (5.30 mL, 61.8 mmol). The reaction was stirred until bubbling ceased (~15 minutes) after which the mixture was heated at 50 °C for five h. The reaction mixture was concentrated *in vacuo* and the residue was redissolved in dry pyridine (80 mL, 0.47 M) followed by addition of 3-aminopyridine (3.75 g, 39.8 mmol) in portions. The pale pink suspension was stirred overnight at room temperature upon which the reaction was quenched with demi-water (200 mL). The resulting precipitate was filtered off, washed with water (3 x 50 mL) and Et_2O (3 x 50 mL) affording **5** as an off-white solid (10.9 g, 30.2 mmol, 81%). R_f = 0.50 (10% MeOH in DCM); IR (neat): 3359, 3221, 3035, 1710, 1670, 1531; ^{1}H NMR: (500 MHz, [D_6]DMSO) δ = 10.42 (s, 1H, H_{arom}), 8.94 (s, 1H, H_{arom}), 8.32 (d, J = 5.4 Hz, 1H, H_{arom}), 8.20 (d, J = 8.6 Hz, 1H, H_{arom}), 7.94 (d, J = 7.9 Hz, 3H, H_{arom}), 7.45 – 7.25

(m, 6H, H_{arom}), 5.06 (s, 2H, CH_2 Cbz), 4.30 (d, J = 6.7 Hz, 2H, CH_2 Arom); ^{13}C NMR: (126 MHz, [D_6]DMSO) δ = 166.2 (C=O CONH), 157.0 (C=O CBz), 145.0 (C_H Arom), 144.4 (C_q Arom), 142.4 (C_H Arom), 137.7 (C_q Arom), 136.4 (C_q Arom), 133.4 (C_q Arom), 128.9 (C_H Arom), 128.4 (C_H Arom), 127.9 (C_H Arom), 127.4 (C_H Arom), 124.1 (C_H Arom), 66.0 (CH_2 CBz), 44.1 (CH_2 Arom); HRMS: *m/z* calcd for [$C_{21}H_{19}N_3O_3$ + H^+]: 362.14992; found: 362.15013.

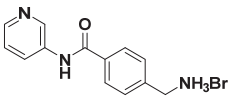

4-(aminomethyl)-*N*-(pyridin-3-yl)benzamide (bromide salt), 6: Compound **5** (6.03 g, 16.7 mmol) was suspended in 33% HBr in acetic acid (90 mL, 0.19 M) and stirred under a dry atmosphere at room temperature for 3 h, after which the precipitate was filtered off and washed with Et_2O (3 x 50 mL), yielding **6** as a white solid (6.36 g, 16.3 mmol, 98%). R_f = 0.20 (20% MeOH, 0.1% Et_3N in DCM); IR (neat): 3121, 3008, 2934, 1681, 1585, 1534); ^{1}H NMR: (500 MHz, CD_3OD) δ 9.62 = (s, 1H, H_{arom}), 8.82 (d, J = 8.8 Hz, 1H, H_{arom}), 8.64 (d, J = 5.8 Hz, 1H, H_{arom}), 8.14 (m, 3H, H_{arom}), 7.68 (d, J = 7.9 Hz, 2H, H_{arom}), 4.26 (s, 2H, CH_2 Arom); ^{13}C NMR: (126 MHz, CD_3OD) δ = 168.0 (C=O $CONH_2$), 140.9 (C_q Arom), 139.2 (C_q Arom), 137.7 (C_H Arom), 135.1 (C_q Arom), 134.1 (C_H Arom), 130.4 (C_H Arom), 129.9 (C_H Arom), 129.9 (C_H Arom), 43.8 (CH_2 Arom); HRMS: *m/z* calcd for [$C_{13}H_{13}N_3O$ + H^+]: 228.11314; found: 228.11323.

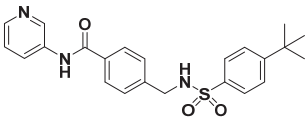

4-((4-(*t*-butyl)phenylsulfonamido)methyl)-N-(pyridin-3-yl)benzamide, 7 (STF-31): To a suspension of **6** (632 mg, 1.62 mmol) in dry pyridine (10 mL, 0.16 M) was added dropwise a solution of 4-(*t*-butyl)benzenesulfonyl chloride (393 mg, 1.69 mmol) in dry MeCN (5 mL, 0.34 M). The bright yellow mixture was stirred overnight under a dinitrogen atmosphere after which it was diluted with EtOAc (100 mL) and transferred to a separatory funnel. The organic layer was washed with 1 M HCl (3 x 25 mL), sat. $NaHCO_3$ (3 x 25 mL) and water (3 x 25 mL) after which it was dried ($MgSO_4$) and concentrated *in vacuo.* Recrystallization from EtOAc/PE afforded the title compound as a fine beige powder (367 mg, 0.87 mmol, 54%). R_f = 0.61 (10% MeOH in DCM); IR (neat): 3121, 2934, 3008, 1681, 1611, 1586, 1534); ^{1}H NMR (500 MHz, [D_6]DMSO) δ = 10.38 (s, 1H, CON*H*), 8.91 (s, 1H, H_{arom}), 8.31 (d, J = 5.0 Hz, 1H, H_{arom}), 8.23 (s, 1H, SO_2N*H*), 8.17 (d, J = 8.4 Hz, 1H, H_{Arom}), 7.86 (d, J = 7.9 Hz, 2H, H_{arom}), 7.69 (d, J = 8.1 Hz, 2H, H_{arom}), 7.55 (d, J = 8.2 Hz, 2H, H_{arom}), 7.43 – 7.35 (m, 4H, H_{arom}), 4.09 (s, 2H, CH_2 Arom), 1.28 (s, 9H, 3 x CH_3 *t*Bu); ^{13}C NMR (126 MHz, DMSO) δ = 165.5 (C=O $CONH_2$), 155.3 (C_q Arom), 142.0 (C_H Arom), 141.8 (C_q Arom), 137.9 (C_q Arom), 135.8 (C_q Arom), 132.9 (C_q Arom), 127.6 (C_H Arom), 127.5 (C_H Arom), 127.3 (C_H Arom), 126.3 (C_H Arom), 125.9 (C_H Arom), 123.5 (C_H Arom), 45.8 (CH_2 Arom), 30.8 (3 x CH_3 *t*Bu); HRMS: *m/z* calcd for [$C_{23}H_{25}N_3O_3S$ + H^+]: 424.16894; found: 424.16987; elemental analysis *calcd* (%): C, 65.23; H, 5.95; N, 9.92; found: C 65.52, H 6.32, N 9.73.

6.4.3 Complex synthesis

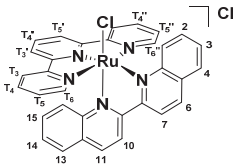

[Ru(tpy)(biq)Cl]Cl, [3]Cl_2: To a solution of Ruthenium dimer [{Ru(tpy)Cl_2 }$_2$].H_2O (199 mg, 0.230 mmol) in 1,2-ethanediol (3 mL, 0.08 M) was added 2,2'-biquinoline (biq) (119 mg, 0.462 mmol) and the mixture was heated at 180 °C for 1 hr after which the solution was allowed to cool down to rt, diluted with EtOH (10 mL) and filtered over Celite to remove any insoluble material. Ethanol was removed *in vacuo* and Et_2O was added to the residue, resulting in a precipitate which was washed with Et_2O (3 x 50 mL) and dried under high vacuum affording a violet microcrystalline solid. (275 mg, 0.416 mmol, 90%). R_f = 0.85 (100/80/20 acetone/water/aq. KPF_6); ^{1}H NMR (500 MHz, CD_3OD) δ = 9.65 (d, *J* = 9.5 Hz, 1H, 1), 8.97 (d, *J* = 8.9 Hz, 1H, 6), 8.91 (d, *J* = 9.3 Hz, 1H, 7), 8.65 (dd, *J* = 14.2, 8.4 Hz, 3H, 10, T_3', T_5'), 8.47 (d, *J* = 8.0 Hz, 1H, T_3, T_3"), 8.30 (dd, *J* = 8.0, 1.8 Hz, 1H, 4), 8.24 (d, *J* = 9.3 Hz, 1H, 11), 8.19 (t, *J* = 8.1 Hz, 1H, T_4'), 7.96 – 7.77 (m, 7H, T_4, T_4", T_6, T_6", 2, 3, 16), 7.44 (ddd, *J* = 8.2, 6.9, 1.3 Hz, 1H, 15), 7.32 (ddd, *J* = 7.3, 5.6, 1.4 Hz, 2H, T_5, T_5"), 7.20 (ddd, *J* = 8.6, 6.9, 1.5 Hz, 1H, 14), 6.80 (d, *J* = 9.0 Hz, 1H, 13); ^{13}C NMR (126 MHz, CD_3OD) δ = 163.2 (C_q Arom), 160.7 (C_q Arom), 160.4 (C_q Arom), 160.0 (C_q Arom), 153.9 (2 x C_H 3, 16) 153.2 (C_q Arom), 152.5 (C_q Arom), 139.8 (C_H 7), 138.8 (C_H T_4, T_4"), 137.7 (C_H 11), 136.8 (C_H T_4'), 132.1 (C_H 14), 131.8 (2 x C_H T_6, T_6"), 131.8 (2 x C_H T_4, T_4"), 130.8 (C_q Arom), 130.4 (2 x C_H 2, 3), 129.9 (1 x C_H 4), 129.7 (C_q Arom), 129.6 (C_H 15), 128.4 (2 x CH T_5, T_5"), 124.9 (C_H 13), 124.9 (2 x C_H T_3, T_3"), 123.9 (2 x CH T_3', T_5'), 121.7 (C_H 10), 121.7 (C_H 6). ^{13}C NMR (126 MHz, CD_3OD) δ = 161.9, 159.4, 159.0, 158.6, 152.5, 151.8, 151.2, 138.4, 137.5, 136.4, 135.5, 130.7, 130.5, 130.4, 129.4, 129.1, 128.6, 128.4, 128.3, 127.0, 123.6, 123.5, 122.6, 120.4, 120.4; HRMS: *m/z* calcd for [$C_{33}H_{23}N_5Cl_2Ru$ – Cl]: 626.06800; found: 626.06891.

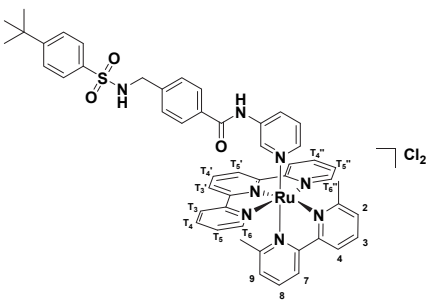

[Ru(tpy)(dmbpy)(STF-31)]Cl_2, [1]Cl_2: To a solution of [Ru(tpy)(dmbpy)Cl]Cl[14] (204 mg, 0,346 mmol) in deoxygenated EtOH/H_2O (10 mL, 2:1, 0.035 M) was added STF-31 (178 mg, 0.420 mmol) and $AgPF_6$ (180 mg, 0.712 mmol) the mixture was stirred at 80 °C for 4 h, after which it was filtered over Celite and concentrated *in vacuo* at 30 °C. The crude product was directly purified over Sephadex LH-20 (acetone). The orange band was collected, the volume reduced to ~10% and a saturated solution of NBu_4Cl in acetone (1 mL) was added. The resulting precipitate was collected by filtration over a Whatman® RC60 membrane filter and subsequently washed with acetone (3 x 50 mL) and Et_2O (3 x 50 mL). Reprecipitation from EtOH/Et_2O afforded the title compound as a microcrystalline red solid (176 mg, 0,174 mmol, 50%). R_f = 0.53 (100/80/20

acetone/water/aq. KPF_6); ^{1}H NMR: (500 MHz, CD_3OD) δ = 8.83 – 8.74 (m, 3H, H_{arom}), 8.72 – 8.64 (m, 2H, H_{arom}), 8.59 (d, J = 8.0 Hz, 1H, H_{arom}), 8.51 (d, J = 8.0 Hz, 1H, H_{Arom}), 8.37 – 8.29 (m, 2H, H_{arom}), 8.27 – 8.18 (m, 3H, H_{arom}), 8.14 (t, J = 7.9 Hz, 1H, H_{arom}), 7.83 (d, J = 7.9 Hz, 1H, H_{arom}), 7.81 – 7.69 (m, 5H, H_{arom}), 7.65 (dt, J = 13.7, 6.6 Hz, 2H, H_{arom}), 7.53 (dd, J = 19.4, 7.1 Hz, 3H, H_{arom}), 7.36 (d, J = 8.2 Hz, 2H, H_{arom}), 7.12 (dd, J = 8.5, 5.5 Hz, 1H, H_{arom}), 7.05 (d, J = 7.6 Hz, 1H, H_{arom}), 4.13 (s, 2H, CH_2 Arom), 2.18 (s, 3H, 1 x CH_3 Arom), 1.56 (s, 3H, 1 x CH_3 Arom), 1.33 (s, 9H, 3 x CH_3 *t*Bu); ^{13}C NMR: (126 MHz, CD_3OD) δ 166.7 (C=O *C*ONH), 165.0 (C_q Arom), 159.3 (C_q Arom), 159.1 (C_q Arom), 158.9 (C_q Arom), 158.8 (C_q Arom), 158.7 (C_q Arom), 158.0 (C_q Arom), 156.1 (C_q Arom), 153.8 (C_H Arom), 152.8 (C_H Arom), 146.6 (C_H Arom), 142.3 (C_q Arom), 142.3 (C_H Arom), 138.8 (C_H Arom), 138.7 (C_H Arom), 138.2 (C_H Arom), 137.9 (C_H Arom), 137.8 (C_q Arom), 132.4 (C_q Arom), 128.7 (C_H Arom), 128.7 (C_H Arom), 128.6 (C_H Arom), 128.4 (C_H Arom), 127.6 (C_H Arom), 127.5 (C_H Arom), 126.9 (C_H Arom), 126.6 (C_H Arom), 125.8 (C_H Arom), 125.6 (C_H Arom), 125.2 (C_H Arom), 124.5 (C_H Arom), 124.2 (C_H Arom), 123.6 (C_H Arom), 122.0 (C_H Arom), 121.7 (C_H Arom), 46.0 (CH_2 Arom), 30.2 (3 x CH_3 *t*Bu), 24.0 (CH_3 Arom), 22.3 (CH_3 Arom); HRMS: *m/z* calcd (%) for [$C_{50}H_{48}N_8O_3RuSCl_2$ – 2Cl]: 471.13013; found: 471.13089; elemental analysis *calcd* (%) for [**1**]Cl_2.4H_2O: C, 55.35; H, 5.20; N, 10.33; found: C, 55.59 H, 5.24 N, 10.28.

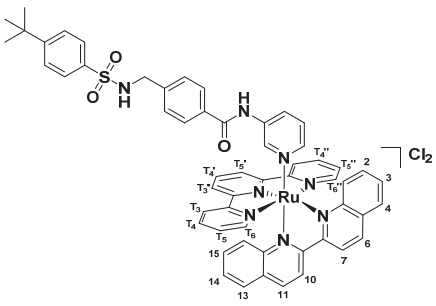

[Ru(tpy)(biq)(STF-31)]Cl_2, [2]Cl_2: To a solution of [Ru(tpy)(biq)Cl]Cl (59.8 mg, 0,0904 mmol) in deoxygenated acetone/H_2O (10 mL, 1:1, 0.009 M) was added STF-31 (75 mg, 0.177 mmol) and $AgPF_6$ (50 mg, 0.198 mmol) and the mixture was heated at 50 °C for 2 h. The purple mixture was filtered hot over Celite, and concentrated *in vacuo* at 30 °C. The crude product was purified over Sephadex LH-20 (methanol). The pink/purple band was collected, concentrated, redissolved in a minimal amount of acetone and precipitated by the addition of 1 mL saturated NBu_4Cl in acetone. The resulting precipitate was collected by filtration over a Whatman® RC60 membrane filter and subsequently washed with acetone (3 x 5 mL) and Et_2O (3 x 5 mL). The precipitate was recovered with MeOH and concentrated, affording the title compound as a purple solid. (43.5 mg, 0,0400 mmol, 44%). R_f = 0.61 (100/80/20 acetone/water/aq. KPF_6); ^{1}H NMR: (500 MHz, CD_3OD) δ = 9.19 (d, J = 8.8 Hz, 1H, H_{arom}), 9.07 (d, J = 8.8 Hz, 1H, H_{arom}), 8.93 (dd, J = 12.7, 8.6 Hz, 2H, H_{arom}), 8.83 – 8.78 (m, 2H, H_{arom}), 8.70 (d, J = 8.0 Hz, 1H, H_{arom}), 8.48 (t, J = 7.1 Hz, 2H, H_{arom}), 8.40 – 8.32 (m, 2H, H_{arom}), 8.21 – 8.08 (m, 2H, H_{arom}), 8.05 – 7.95 (m, 2H, H_{arom}), 7.89 (d, J = 8.0 Hz, 1H, H_{arom}), 7.81 – 7.69 (m, 4H, H_{arom}), 7.67 (d, J = 8.4 Hz, 2H, H_{arom}), 7.59 – 7.48 (m, 4H, H_{arom}), 7.45 (dd, J = 24.4, 6.1 Hz, 2H, H_{arom}), 7.41 – 7.28 (m, 5H, H_{arom}), 6.99 (dd, J = 8.5, 5.7 Hz, 1H, H_{arom}), 6.82 (d, J = 8.8 Hz, 1H, H_{arom}), 4.12 (s, 2H, CH_2 Arom), 1.33 (s, 9H, 3 x CH_3 *t*Bu); ^{13}C NMR: (126 MHz, CD_3OD) δ = 168.0 (C=O *C*ONH), 161.8

(C_q Arom), 160.7 (C_q Arom), 160.1 (C_q Arom), 160.0 (C_q Arom), 159.6 (C_q Arom), 157.5 (C_q Arom), 152.2 (C_q Arom), 151.2 (C_q Arom), 148.2 (C_H Arom), 143.9 (C_H Arom), 143.2 (C_H Arom), 141.0 (C_H Arom), 140.3 (C_H Arom), 140.2 (C_H Arom), 140.0 (C_H Arom), 139.4 (C_q Arom), 139.1 (C_q Arom), 138.3 (C_H Arom), 133.8 (C_q Arom), 132.7 (C_H Arom), 132.4 (C_H Arom), 131.7 (C_q Arom), 131.4 (C_H Arom), 130.8 (C_H Arom), 130.4 (C_H Arom), 130.0 (C_H Arom), 130.0 (C_q Arom), 129.8 (C_H Arom), 129.8 (C_H Arom), 129.0 (C_H Arom), 128.8 (C_H Arom), 127.9 (C_H Arom), 127.5 (C_H Arom), 126.0 (C_H Arom), 125.8 (C_H Arom), 125.2 (C_H Arom), 124.7 (C_H Arom), 122.5 (C_H Arom), 122.3 (C_H Arom), 47.3 (CH_2 Arom), 31.5 (3 x CH_3 Arom); HRMS: *m/z* calcd for $[C_{56}H_{48}N_8O_3RuSCl_2 - 2Cl]$: 507.13013; found: 507.13098; elemental analysis *calcd* (%) for [**2**]Cl_2.$4H_2O$: C, 58.13; H, 4.88; N, 9.68; found: C, 58.14 H, 4.78 N, 9.53.

6.4.4 Photosubstitution quantum yield determination

3.00 mL of [**1**]Cl_2 (6.83 x 10^{-5} M) or [**2**]Cl_2 (4.10 x 10^{-5} M) in demiwater was deoxygenated for 15 minutes with nitrogen after which it was irradiated while the solution was kept at constant temperature (25 or 37 °C). During this period UV-vis spectra were recorded on a Varian Inc. Cary 50 UV-vis spectrometer with an interval of 30 seconds until 630 seconds. ESI-MS spectra were recorded after the irradiation experiment to confirm the formation of the aqua species $[Ru(tpy)(dmbpy)(OH_2)]^{2+}$ and $[Ru(tpy)(biq)(OH_2)]^{2+}$. The quantum yield of photosubstitution was calculated as described before[20] with the following modification: The photon flux was extrapolated from the average ratio between the photon flux determined by ferrioxalate actinometry[29] and the theoretical photon flux of the same family of LEDs (413, 450 and 490) at a given power density and was calculated 1.32 x 10^{-7} mol s^{-1} at 625 nm. For the photosubstitution of **[1]Cl_2** 500 and 410 nm were used as reference wavelengths, with ε_{500} = 2.2 x 10^3 M cm^{-1} and ε_{410} = 6.2 x 10^3 M cm^{-1} with ε_{500} = 5.4 x 10^3 M cm^{-1} and ε_{500} = 3578 M cm^{-1} for $[Ru(tpy)(dmbpy)(H_2O)]Cl_2$. For the photosubstitution of **[2]Cl_2** 550 and 500 nm were used as reference wavelengths, with ε_{550} = 6.9 x 10^3 M cm^{-1} and ε_{500} = 7.1 x 10^3 M cm^{-1} with ε_{550} = 9.9 x 10^3 M cm^{-1} and ε_{500} = 5.8 x 10^3 M cm^{-1} for $[Ru(tpy)(biq)H_2O]Cl_2$.

6.4.5 Singlet oxygen ($^1O_2$) quantum yield measurements

The setup, measurement and calculation were carried out as described in general appendix I.1.1 with the following modifications: Irradiation was carried out using a red laser (635 nm) with methylene blue as a reference in CD_3OD (Φ_Δ = 0.52)[30] at 293 K.

6.4.6 UV-vis evolution spectrum in a 96-well plate in DMSO and OptiMEM® media

Compounds [**1**]Cl_2 and [**2**]Cl_2 were dissolved in OMEM (OptiMEM® without phenol red, supplemented with 0.2% (P/S), 0.9% v/v Glutamine-S and 2.0% FCS) + 10% DMSO and pure DMSO. In order to prevent light-scattering occurring from the precipitation of STF-31 a higher concentration of DMSO was used. Compounds were transferred to a 96-well plate,

irradiated at different intervals (t = 0, 1, 2, 3, 4, 5, 10 and 15 minutes) with red light (628 ± 19 nm, 34.4 ± 1.7 mW · cm^{-2}), followed by a read-out at a M1000 Tecan® reader. Spectra were plotted using Origin Pro 9.1 and the baseline was subtracted to correct for baseline drifting.

6.4.7 Log $P_{o/w}$ determination

The partition coefficient between *n*-octanol and water (log $P_{o/w}$) were determined following to the method described in appendix I.2.3.

6.4.8 Stability in OptiMEM ®media 48 hours

Compound [**1**]Cl_2 and [**2**]Cl_2 (c = 1.0 x 10^{-4} and 1.1 x 10^{-4} M respectively) were dissolved in OMEM complete (OptiMEM without phenol red, supplemented with 0.2% (P/S), 0.9% v/v Glutamine-S and 2.0% FCS). Absorption spectra were recorded in Varian Inc. Cary 50 UV-vis spectrometer over 48 hours with an interval of 15 minutes while maintaining the temperature at 37 °C. After this time period samples were frozen solid using liquid nitrogen, lyophilized and redissolved in methanol. ESI-MS spectra were recorded to confirm the major species to be $[Ru(tpy)(dmbpy)Cl]^+$ (554.1 calcd, 554.1 found) and $[\mathbf{2}]^{2+}$ (507.1 calcd., 506.9 found) for [**1**]Cl_2 and [**2**]Cl_2 respectively.

6.4.9 Biology

Experimental details of cell culturing, cytotoxicity and cell irradiation under normoxia and hypoxia, NBDG-uptake, and NAMPT inhibition can be found in the appendix (V.2).

References

[1] A. D. Gujar, S. Le, D. D. Mao, D. Y. Dadey, A. Turski, Y. Sasaki, D. Aum, J. Luo, S. Dahiya, L. Yuan, K. M. Rich, J. Milbrandt, D. E. Hallahan, H. Yano, D. D. Tran, A. H. Kim, *P Natl Acad Sci USA* **2016**, *113*, E8247-E8256.

[2] a). J. A. Khan, X. Tao, L. Tong, *Nat Struct Mol Biol* **2006**, *13*, 582-588; b). C. A. Lyssiotis, L. C. Cantley, *Clin Cancer Res* **2014**, *20*, 6-8.

[3] B. Tan, D. A. Young, Z. H. Lu, T. Wang, T. I. Meier, R. L. Shepard, K. Roth, Y. Zhai, K. Huss, M. S. Kuo, J. Gillig, S. Parthasarathy, T. P. Burkholder, M. C. Smith, S. Geeganage, G. Zhao, *J Biol Chem* **2013**, *288*, 3500-3511.

[4] T. S. Zabka, J. Singh, P. Dhawan, B. M. Liederer, J. Oeh, M. A. Kauss, Y. Xiao, M. Zak, T. Lin, B. McCray, N. La, T. Nguyen, J. Beyer, C. Farman, H. Uppal, P. S. Dragovich, T. O'Brien, D. Sampath, D. L. Misner, *Toxicol Sci* **2015**, *144*, 163-172.

[5] a). D. Crespy, K. Landfester, U. S. Schubert, A. Schiller, *Chem Commun* **2010**, *46*, 6651-6662; b). C. Mari, V. Pierroz, S. Ferrari, G. Gasser, *Chem Sci* **2015**, *6*, 2660-2686; c). U. Schatzschneider, *Eur J Inorg Chem* **2010**, *2010*, 1451-1467; d). N. J. Farrer, L. Salassa, P. J. Sadler, *Dalton Trans* **2009**, 10690-10701; e). A. Presa, R. F. Brissos, A. B. Caballero, I. Borilovic, L. Korrodi-Gregorio, R. Perez-Tomas, O. Roubeau, P. Gamez, *Angew Chem Int Ed* **2015**, *54*, 4561-4565.

[6] T. Respondek, R. Sharma, M. K. Herroon, R. N. Garner, J. D. Knoll, E. Cueny, C. Turro, I. Podgorski, J. J. Kodanko, *ChemMedChem* **2014**, *9*, 1306-1315.

[7] a). E. M. Rial Verde, L. Zayat, R. Etchenique, R. Yuste, *Front Neural Circuits* **2008**, *2*, 2; b). B. S. Howerton, D. K. Heidary, E. C. Glazer, *J Am Chem Soc* **2012**, *134*, 8324-8327; c). S. Betanzos-Lara, L. Salassa, A. Habtemariam, O. Novakova, A. M. Pizarro, G. J. Clarkson, B. Liskova, V. Brabec, P. J. Sadler, *Organometallics* **2012**, *31*, 3466-3479; d). A. Habtemariam, C. Garino, E. Ruggiero, S. Alonso-de Castro, J. Mareque Rivas, L. Salassa, *Molecules* **2015**, *20*, 7276-7291.

[8] a). P. Anstaett, V. Pierroz, S. Ferrari, G. Gasser, *Photobiol Sci* **2015**, *14*, 1821-1825; b). L. Zayat, M. G. Noval, J. Campi, C. I. Calero, D. J. Calvo, R. Etchenique, *Chembiochem* **2007**, *8*, 2035-2038; c). T. Joshi, V. Pierroz, C. Mari, L. Gemperle, S. Ferrari, G. Gasser, *Angew Chem Int Ed* **2014**, *53*, 2960-2963.

[9] D. E. Dolmans, D. Fukumura, R. K. Jain, *Nat Rev Cancer* **2003**, *3*, 380-387.

[10] P. Avci, A. Gupta, M. Sadasivam, D. Vecchio, Z. Pam, N. Pam, M. R. Hamblin, *Semin Cutan Med Surg* **2013**, *32*, 41-52.

[11] S. L. Hopkins, B. Siewert, S. H. Askes, P. Veldhuizen, R. Zwier, M. Heger, S. Bonnet, *Photobiol Sci* **2016**, *15*, 644-653.

[12] a). A. Li, R. Yadav, J. K. White, M. K. Herroon, B. P. Callahan, I. Podgorski, C. Turro, E. E. Scott, J. J. Kodanko, *Chem Commun* **2017**, *53*, 3673-3676; b). J. D. Knoll, B. A. Albani, C. B. Durr, C. Turro, *J Phys Chem A* **2014**, *118*, 10603-10610.

[13] H. Yin, M. Stephenson, J. Gibson, E. Sampson, G. Shi, T. Sainuddin, S. Monro, S. A. McFarland, *Inorg Chem* **2014**, *53*, 4548-4559.

[14] A. Bahreman, B. Limburg, M. A. Siegler, E. Bouwman, S. Bonnet, *Inorg Chem* **2013**, *52*, 9456-9469.

[15] a). D. J. Adams, D. Ito, M. G. Rees, B. Seashore-Ludlow, X. Puyang, A. H. Ramos, J. H. Cheah, P. A. Clemons, M. Warmuth, P. Zhu, A. F. Shamji, S. L. Schreiber, *Acs Chem Biol* **2014**, *9*, 2247-2254; b). P. S. Dragovich, K. W. Bair, T. Baumeister, Y. C. Ho, B. M. Liederer, X. Liu, Y. Liu, T. O'Brien, J. Oeh, D. Sampath, N. Skelton, L. Wang, W. Wang, H. Wu, Y. Xiao, P. W. Yuen, M. Zak, L. Zhang, X. Zheng, *Bioorg Med Chem Lett* **2013**, *23*, 4875-4885; c). E. M. Kropp, B. J. Oleson, K. A. Broniowska, S. Bhattacharya, A. C. Chadwick, A. R. Diers, Q. Hu, D. Sahoo, N. Hogg, K. R. Boheler, J. A. Corbett, R. L. Gundry, *Stem Cell Transl Med* **2015**, *4*, 483-493.

[16] a). D. A. Chan, P. D. Sutphin, P. Nguyen, S. Turcotte, E. W. Lai, A. Banh, G. E. Reynolds, J. T. Chi, J. Wu, D. E. Solow-Cordero, M. Bonnet, J. U. Flanagan, D. M. Bouley, E. E. Graves, W. A. Denny, M. P. Hay, A. J. Giaccia, *Sci Transl Med* **2011**, *3*, 1-9; b). M. Bonnet, J. U. Flanagan, D. A. Chan, A. J. Giaccia, M. P. Hay, *Bioorg Med Chem* **2014**, *22*, 711-720; c). D. Kraus, J. Reckenbeil, M. Wenghoefer, H. Stark, M. Frentzen, J. P. Allam, N. Novak, S. Frede, W. Gotz, R. Probstmeier, R. Meyer, J. Winter, *Cell Mol Life Sci* **2016**, *73*, 1287-1299.

[17] D. C. Marelius, S. Bhagan, D. J. Charboneau, K. M. Schroeder, J. M. Kamdar, A. R. McGettigan, B. J. Freeman, C. E. Moore, A. L. Rheingold, A. L. Cooksy, D. K. Smith, J. J. Paul, E. T. Papish, D. B. Grotjahn, *Eur J Inorg Chem* **2014**, 676-689.

[18] A. J. Gottle, F. Alary, M. Boggio-Pasqua, I. M. Dixon, J. L. Heully, A. Bahreman, S. H. Askes, S. Bonnet, *Inorg Chem* **2016**, *55*, 4448-4456.

[19] A. Bahreman, B. Limburg, M. A. Siegler, E. Bouwman, S. Bonnet, *Inorg Chem* **2013**, *52*, 9456-9469.

[20] A. Bahreman, J. A. Cuello-Garibo, S. Bonnet, *Dalton Trans* **2014**, *43*, 4494-4505.

[21] V. Vichai, K. Kirtikara, *Nat Protocols* **2006**, *1*, 1112-1116.

[22] J. P. Cosse, C. Michiels, *Anti-cancer agents in medicinal chemistry* **2008**, *8*, 790-797.

[23] a). C. Xintaropoulou, C. Ward, A. Wise, H. Marston, A. Turnbull, S. P. Langdon, *Oncotarget* **2015**, *6*, 25677-25695; b). T. Matsumoto, S. Jimi, K. Migita, Y. Takamatsu, S. Hara, *Leukemia Res* **2016**, *41*, 103-110.

[24] J. Park, H. Y. Lee, M. H. Cho, S. B. Park, *Angew Chem Int Ed* **2007**, *46*, 2018-2022.

[25] S. C. Hsu, R. S. Molday, *J Biol Chem* **1991**, *266*, 21745-21752.

[26] C. Zou, Y. Wang, Z. Shen, *J Biochem Bioph Meth* **2005**, *64*, 207-215.

[27] L. Ma, R. Wang, Y. Nan, W. Li, Q. Wang, F. Jin, *Int J Oncol* **2016**, *48*, 843-853.

[28] S. S. Dhillon, T. L. Demmy, S. Yendamuri, G. Loewen, C. Nwogu, M. Cooper, B. W. Henderson, *J Thorac Oncol* **2016**, *11*, 234-241.

[29] C. G. Hatchard, C. A. Parker, *Proc R Soc A* **1956**, *235*, 518-536.

[30] C. Tanielian, C. Wolff, *J Phys Chem* **1995**, *99*, 9825-9830.